JCTC Journal of Chemical Theory and Computation

Merging Implicit with Explicit Solvent Simulations: Polyethylene Glycol

Alok Juneja,[†] Jorge Numata,[†] Lennart Nilsson,[‡] and Ernst Walter Knapp*,[†]

Freie Universität Berlin, Institute of Chemistry & Biochemistry, Fabeckstr. 36a, D-14195 Berlin, Germany and Centre for Biosciences, Department of Biosciences and Nutrition, Karolinska Institutet, SE-141 83 Huddinge, Sweden

Received February 6, 2010

Abstract: We constructed an accurate polyether force field for implicit solvent (IS) molecular dynamics (MD) simulations that matches local and global conformations of 1,2-dimethoxy-ethane (DME) and polyethylene glycol (PEG), respectively. To make appropriate force field adjustments for IS models of PEG, we used long-term MD simulation data of 1 μs in explicit solvent (ES) based on the most recent CHARMM35 ether force field that includes adjustments for PEG in explicit water. In IS models, competition of attractive van der Waals (vdW) interactions between solute−solute and solute−solvent atom pairs is often not considered explicitly. As a consequence, the attractive vdW interactions between solute atom pairs that remain in IS models explicitly can yield equilibrium structures that are too compact. This behavior was observed in the present study comparing MD simulation data of the DME and PEG ES model with corresponding IS models that use generalized Born (GB) electrostatics combined with positive surface energy terms favoring compact structures. To regain balance of attractive vdW interactions for IS models, we considered the IS generalized Born with simple switching (GBSW) model in detail, where we turned off surface energy terms and reduced attractive vdW interactions to 90%, or we used alternatively even slightly negative surface energies. However, to obtain quantitatively the same local and global distributions of PEG conformers as in ES, we needed additional force field adjustments involving torsion potentials and 1−4 and 1−5 atom pair Coulomb interactions. This CHARMM ether force field, specifically optimized for IS simulation conditions, is equally valid for dimeric and polymeric ethylene glycol. To explore the conformational space of PEG with MD simulations, an IS GBSW model requires 2 orders of magnitude less CPU time than the corresponding ES model. About a factor of 5 of this gain in efficiency is due to the lack of solvent viscosity in IS models.

Introduction

The behavior of molecules in solution depends fundamentally on the balance between solute−solute, solute−solvent, and solvent−solvent interactions. The type of solvent used determines the solvation and association behavior of molecules as well as their protonation and redox states in the case of titratable or redox-active molecules and their conformations in the case of larger flexible molecules. The native structure of biological macromolecules and in particular of proteins is governed by interactions with water.[1,2] Biological macromolecules need to be under physiological conditions (i.e., to be in aqueous solution at specific temperatures, pH's, and ionic strengths) to adopt their native structure, which is a prerequisite to function appropriately.[3−7] Binding strengths of drugs, substrates, and inhibitors to proteins are strongly influenced by water.[2,8−10] Also, conformational dynamics and the function of proteins is solvent

* Corresponding author phone: 0049-30-838-54387; fax: 0049-30-838-56921; e-mail: knapp@chemie.fu-berlin.de.

[†] Freie Universität Berlin.

[‡] Karolinska Institutet.

10.1021/ct100075m
Published on Web 05/12/2010

controlled.[11−13] On the other hand, the neighborhood of a protein surface influences also the behavior of the surrounding water. It restricts conformational variability of water, leading to reduced entropy,[12,14,15] and slows down its dynamics by about a factor of 2 to 4.[16,17] Thus, modeling and simulation of structure and dynamics of molecules and their interactions in solutions generally requires the consideration of interactions with solvent molecules in atomic detail. This is why, in approaches using molecular dynamics (MD) simulations, the considered molecules need to be embedded sufficiently well in a solvent environment.

In conventional MD simulations of solute−water systems, water molecules are described explicitly in atomic detail employing an atom-based molecular force field. Such MD simulations involve routinely a large number of atoms, where most of them belong to solvent molecules. Even in the best case, the computational costs of such molecular systems increase faster than linearly with the number of atoms, making MD simulations with explicit solvent (ES) models rather expensive.

Different procedures have been applied to reduce the CPU time required for MD simulations. One focus is to use implicit solvent (IS) models for water,[18−26] which diminish the number of atoms to be considered enormously. An additional efficiency bonus of IS models is the absence of solvent viscosity. As a consequence, the actually used elementary time step of MD simulations with an IS model can in reality correspond to a larger time interval, as has been found in IS generalized Born using molecular volume (GBMV) MD simulations when a low friction constant was used.[27] This would allow exploration of the conformational space of a solute molecule in less simulation time but bears the disadvantage that the dynamics are unrealistically fast. Water interacts with solute molecules in three ways: two direct and one indirect type of interaction. The former two are electrostatic[28] and van der Waals (vdW) interactions;[12] the latter is due to the hydrophobic effect.[2,13,15,29−31] The influence of hydrogen bonds (H-bonds) is generally accounted for by a suitable combination of electrostatic and vdW interactions.

Solvent modeled as explicit water screens Coulomb (and also vdW) interactions between solute atoms and competes with the direct solute−solute atom pair interactions (Coulomb as well as vdW). In an IS model, the solute−solvent electrostatic interactions is approximated using a dielectric continuum with large dielectric constant for the solvent ($\varepsilon = 80$ for water), while the solute atomic partial charges are embedded in a dielectric cavity of a small dielectric constant (generally $\varepsilon = 1$). In a simplified approach, the electrostatic boundary between a low and high dielectric medium in an IS model can be approximated by the surface separating the vdW solute volume (given by the merged volumes of solute atoms) from the solvent, which is used by GBSW.[32−34] More elaborate procedures use the molecular surface as in GBMV.[35,36] In fast analytical continuum treatment of solvation (FACTS),[37] still another procedure to effectively generate the interface between solute and solvent is used, which is guided by the principle to save CPU time.

In dielectric continuum models, the solute atomic partial charges interact with virtual surface charges induced at the solute−solvent boundary. The corresponding electrostatic energies can be evaluated with the Poisson or for nonvanishing ionic strength with the Poisson−Boltzmann equation.[22,38,39] Since solving the Poisson equation at each time step of MD simulations slows down such simulations considerably, more approximate electrostatic models are used instead. These are, for instance, the generalized Born approximation (GB)[40] or even more simplifying approaches that use distance dependent dielectric constants and neutralized charged groups.[41−44] Although the continuum dielectric medium models explicit electrostatic solute−solvent interactions generally faithfully, it was occasionally observed that solute−solute H bonds and salt bridges are too persistent in the IS model with GB.

In addition to the electrostatic energy contributions, IS force fields contain a nonpolar energy term that accounts for the entropic costs for water to be in contact with the surface of a solute. In touch with the surface of a solute, a water molecule can no longer adopt as many different H-bond patterns as in bulk water. This goes along with a loss of entropy of these water molecules, the so-called hydrophobic effect. Consequently, water has positive contact energy with solute molecules forcing different solute molecules to aggregate and individual solute molecules to assume a compact conformation with a minimal surface. This nonpolar contribution to solvation free energy is generally assumed to be directly proportional to the solvent accessible surface area.[45−47] In MD simulations with the IS model, the hydrophobic effect is normally accounted for by an artificial energy term that is proportional to the solvent exposed solute surface[45−47] with a proportionality constant γ varying between 5 and 40 cal/(mol Å^2).[33,48−51] There have been a number of efforts in recent times to advance IS models[23,24,38,42,43] to simulate dynamics of biomolecules efficiently and to come close to results of computationally more expensive conventional MD simulations with an ES model. However, some GB implementations have the tendency to become inefficient for large molecules.

IS models were also optimized to compute solvation energies efficiently.[52−54] There, it was found that electrostatic models combined with surface energy alone is not appropriate and must be supplemented by a volume term accounting for solvent cavity formation.[52] Here, we study the energetics of 1,2-dimethoxy-ethane (DME) and polyethylene glycol (PEG) conformers in an implicit solvent. Since their volumes practically do not vary with the conformers, these optimized IS models are not applicable in our case.

But there is still another artificial effect, which is generally present in IS models. In explicit water simulations (and also in real molecular systems), the attractive solute−solute and solute−solvent vdW interactions compete with each other and thus balance the composition of solute and solvent atoms in the neighborhood of solutes. In the absence of ES, only the attractive solute−solute vdW interactions are left, and as a result the neighborhood of solute molecules is unbalanced. These solute−solute interactions occur between atoms of different solute molecules (intermolecular) but also between atoms of the same solute molecule (intramolecular).

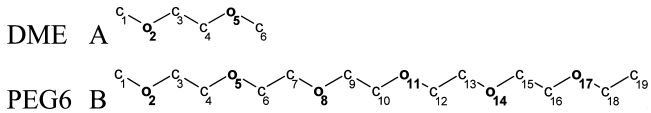

Figure 1. Schematic structure representations of DME (A) and PEG6 (B). Atoms are numbered to refer to specific numbering used in the text.

Removing the solvent molecules, the solute molecules interact differently. Since all atoms are subject to the mutual attractive vdW interactions, one observes for MD simulations in the absence of solvent, aggregation of different solute molecules and for flexible solute molecules also self-aggregation, leading to solute conformers which are too compact. The influence of solute−solvent vdW interactions on molecular solvation energies, ligand binding, and protein docking was discussed many times. However, to the best of our knowledge, it was first pointed out in ref 55 that this effect can also influence molecular conformations significantly. An IS force field including the effect from the solute−solvent vdW interactions appropriately by using a volume term was recently developed and applied to proteins.[56]

The hydrophobic effect[13,15,29−31] is based on the entropy content of the water structure, which assumes a maximum for undisturbed bulk water. While the hydrophobic effect has a physical basis, the mutual attraction of solute molecules in IS models, where attractive vdW interactions are not balanced, is an artifact. The hydrophobic effect causes an effective attraction between different solute molecules and in the case of flexible solute molecules also between atoms of the same solute molecule. It is properly considered in explicit water MD simulations[16,57] and is for instance the driving force of protein folding.[6,7,12] In implicit water simulations with vanishing surface energy, the effective attractive hydrophobic interaction between solute molecules is absent, while conversely the lack of balance in the attractive vdW interactions between solute−solute and solute−solvent contacts leads to an artificial attraction between solute molecules. Hence, under these conditions of an IS model, these two effects partially compensate each other.

Hence, in an IS model, proper tuning is required for the surface energy replacing the hydrophobic effect and the strength of the unbalanced vdW attractions. For similar reasons, it may be necessary to adjust Coulomb interactions for specific atom pairs of the solute to compensate for the absence of explicit H bonds with water molecules, which may have not been considered appropriately by the continuum electrostatic approach. Similar, more subtle effects can be due to a specific H-bond pattern between solute and water molecules, which may stabilize specific solute conformations and thus change the equilibrium distribution between them. As we will see, to account for all these effects appropriately, we need to adjust not only specific atom pair Coulomb interactions but also specific torsion potentials.

As a model system, we will study polyethylene glycol (PEG)[58,59] involving the ethylene glycol repeat unit (−CH_2−CH_2−O−) (Figure 1). Crystallized and amorphous PEG adopt predominantly helix-like conformers (Figure 2).[60,61] They involve the most prevalent local structure TGT (see Figure S1, Supporting Information) found in 1,2-dimethoxy-ethane (DME) and PEG. *Ab initio* quantum chemical calculations of DME, which include solvent effects by continuum electrostatics[62] as well as MD simulations with umbrella sampling in explicit water,[63] indicate that DME prefers the TGT conformer, which is also evident from Raman,[64] IR,[65] and NMR studies.[66] The helical structure of PEG is stabilized by water bridges between nearest neighbor oxygen atoms in PEG. This has been reported by NMR,[67] the *ab initio* quantum chemical method,[68] and MD simulation[69−71] studies.

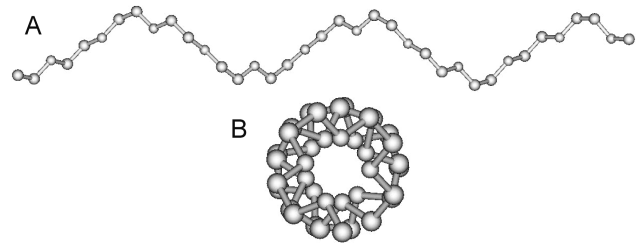

Figure 2. Side (A) and top (B) views of the PEG helix conformer composed of 12 monomer units in local TGT conformations comprising two helix turns. TGT is the most dominant local structure of PEG as well as of DME (see Figures S1 and S2 of the Supporting Information).

PEG is water-soluble, is nontoxic, degrades slowly by metabolic enzymes, and possesses low immunogenicity.[72,73] Therefore, it is widely used as an excipient in different pharmaceutical formulations, foods, and cosmetics.[74,75] PEG is also used as a precipitant agent for protein crystallization.[76] Being flexible and water-soluble, PEG can be used to create high osmotic pressure.[77,78] Coating gene therapy vectors with PEG reduces innate immune responses.[79] Self-assembled monolayers on a gold surface resist protein adsorption from aqueous solutions, if terminated with PEG.[80−82] PEG is of interest for the pharmaceutical industry to encapsulate drugs in nanoparticle structures or dendrimers made of PEG based polymeric material.[75,83−86] It can also be used to connect ligands serving as drugs to form dimeric or even multimeric ligands to enhance drug activity by the multivalent binding effect.[87,88] In multivalent ligand binding, the chain entropy of PEG plays a key role in understanding the effect quantitatively. So far, only a simple Gaussian chain model was used to describe the influence of the PEG linker on bivalent ligand binding.[89,90]

Because of the importance of PEG, it was the focus of many experimental[81,91] and computational studies.[71] Recently, the PEG force field parameters[92,93] for explicit water MD simulations were optimized in CHARMM.[94,95] The present study on IS generalized Born with simple switching (GBSW)[32−34] models uses results of MD simulations with ES based on this improved force field as a reference. Here, we like to demonstrate how large deviations in local and global conformational features of PEG can be, if one uses state of the art IS models like GBSW[32−34] for a flexible molecule, and what one has to change to obtain a faithful force field for IS GBSW MD simulations. We also try to show for DME and PEG to what extent two more GB based IS models (GBMV[35,36] and FACTS[37]) implemented in

CHARMM[94,95] may yield MD simulation data deviating from data obtained with corresponding ES models.

Methods

General Considerations. In the recent years, much effort was placed in the development of theoretical models explaining the conformational preference of 1,2-dimethoxy-ethane (DME).[58] For this purpose, specialized classical force field parameters for MD simulations of DME and PEG were developed[96,97] and applied,[98,99] indicating the existence of specific DME conformers in the liquid phase. Recently, the CHARMM force field has been complemented with parameters for ether compounds,[92] which were further adjusted in CHARMM35[93] using DME Raman spectra.[64]

The DME structure can be characterized by three dihedral angles defining the local arrangement of a set of four covalently connected atoms (C−O−C−C, O−C−C−O, and C−C−O−C). Each of the torsion angles can be in one of the three possible torsion angle intervals, which are centered around 180°, called the trans (T) conformer, or around +60° or −60° corresponding to the two possible gauche (G, G′) conformers. In MD simulations with the ES model, DME adopts a mixture of mainly four conformers, which ordered with decreasing population are TGT, TGG′, TGG, and TTT (see Figures S1 and S2 of the Supporting Information and the insert of Figure 4A). These DME conformers have been observed in various solvents like water,[100] methanol, and carbon tetrachloride.[101] Among these four principal conformers, it has been noticed that TGT has the lowest free energy. In experiments,[100,101] one observes an interesting inverse correlation between the gauche C−C bond and C−O bond populations, which is prevalent in DME and PEG chains and thus corroborates the choice of DME as a model compound to adjust the PEG force field.[93]

Inspired by the Born equation to compute solvation energies of ions,[102] a number of generalized Born (GB) models[33,36,37,40,49,50,103−105] have been developed in the past years. In GB models, the effective nonpolar interactions related to the hydrophobic effect are generally proportional to the solvent accessible surface area (SA).[106] In the actual CHARMM force field, version 35 (CHARMM35),[93] the GBSW[32−34] module for IS MD simulations uses as a default value the proportionality constant $\gamma = 30$ cal/(mol Å^2) for the surface energy term.

To optimize an IS force field for PEG, we considered the GBSW[32−34] model in detail to evaluate the electrostatic interactions as implemented in CHARMM combined with the ES ether force field parametrization of CHARMM35.[93] To probe the generalities of our results found with the GBSW[32−34] model, we also explored two more GB models available in CHARMM (GBMV[35,36] and FACTS[37]). Although we did not consider the GB models in AMBER[107,108] explicitly, their parametrization is qualitatively similar to GB models considered in the present study, such that we expect analogue behavior.

Henceforth, we refer to MD simulations using CHARMM35 with the TIP3P water model[109] as an explicit solvent (ES) model and in the absence of a solvent as described above with default CHARMM35 parametrization as the IS GBSW model with a positive surface energy. The different IS GBSW models considered in the present study are labeled by additional information where they deviate from the default CHARMM35 parameter settings. For the other two GB models (GBMV and FACTS) considered here, we varied the surface energy only. The computations based on the IS GBMV model use the CHARMM35 force field with the recent adjustments for PEG,[93] while the IS FACTS model is based on the CHARMM22[95] force field.

Scaling CHARMM Interactions for Implicit Solvent Simulations. The polyether torsion potentials $V_{O-C-C-O}(\phi)$ and $V_{C-O-C-C}(\phi)$ describing the rotation barrier for the C−C and O−C bonds, respectively, were for explicit solvent simulations optimized yielding in units of kcal/mol

$$V_{O-C-C-O}(\phi) = 0.59(1 + \cos(\phi - \pi)) + 1.16(1 + \cos(2\phi)) \quad (1a)$$

$$V_{C-O-C-C}(\phi) = 0.57(1 + \cos(\phi)) + 0.29(1 + \cos(2\phi)) + 0.43(1 + \cos(3\phi)) \quad (1b)$$

In order to match the torsion angle distributions between ES and IS GBSW model simulations, the parameter of the first term in $V_{O-C-C-O}(\phi)$ was increased from 0.59 to 1.09, while the parameter of the second term in $V_{C-O-C-C}(\phi)$ was reduced from 0.29 to 0.20.

Furthermore, we varied the surface energy term described by the surface tension coefficient γ,[21,110] whose value is proposed to be 30 cal/(mol Å^2)[32,33] in the CHARMM35 IS force field. We also varied the attractive r^{-6} term of the LJ atom-pair interactions. Fine tuning of the energy function of the IS GBSW model required also a change in the Coulomb interactions of the 1−4 atom pairs and of the 1−5 O−H (e.g., O_2-H_6 and O_5-H_1 where the subscript at H refer to the carbon atom to which the hydrogen atom is attached to, see Figure 1) atom pairs.

MD Simulation Protocols. The program CHARMM was used to prepare the ES MD simulation setup with the CHARMM35 ether force field.[93] The TIP3P model[109,111] was used for water. The long-term MD simulations were performed by NAMD.[112] These were 0.1 μs for DME with 199 TIP3P water and 1 μs for PEG6 with 1477 TIP3P water. All parameters and conditions for NAMD were the same as for CHARMM. The temperature was controlled by Langevin thermostat with friction coefficient $\beta = 2$ ps^{-1}, and electrostatic interactions were evaluated using the particle mesh Ewald method.[113] The first 1 ns was discarded to allow for equilibration. Atomic coordinates were saved every 0.2 ps time step. More details on the ES simulation conditions are given in the Supporting Information.

For the three different IS models, MD simulations were carried out with CHARMM35 using the modules GBSW,[32−34,104] GBMV,[35,36] and FACTS.[37] A canonical NVT ensemble was used maintaining the temperature at 300 K with the Nose−Hoover thermostat.[115,116] For GBSW and GBMV, the ether force field[93] was used. To define the electrostatic boundary, GBSW used the vdW surface with optimized atomic Born radii,[114] GBMV used the molecular surface, while FACTS used the solvent accessible surface

area approach. For DME and PEG6 MD, simulations of 100 and 400 ns (200 ns for GBMV) were performed, respectively. Atomic coordinates are saved every 0.2 ps. More details on the simulation conditions are given in the Supporting Information.

Comparison of MD Simulation Data of Explicit and Implicit Solvent Models. To compare the behavior of the DME and PEG force fields using the ES and the IS GBSW models, we considered specific atom pair distance distributions, which were evaluated with standard histogram techniques using the conformers from MD simulation data. The torsion potentials of the IS GBSW models for DME and PEG were optimized by comparing the corresponding torsion potentials. These were obtained by first evaluating the probability distribution of the torsion angles from the conformers of the MD simulation data by a histogram method. These probability distributions were then transformed to free energies by taking the negative logarithm of these probabilities and multiplying them by k_BT with $T =$ 300 K.

How efficient MD simulations explore the space of PEG conformers is found out by observing how the end-to-end atom pair distance distributions $g^{(t)}(x)$ evolve with the total time span t used for the ensemble averages. A suitable quantity to measure how fast the limit distribution $g^{(\infty)}(x)$ of the ensemble is approached with the MD simulation time is the integral of the square deviation

$$[\Delta g^{(t)}]^2 = \int [g^{(t)}(x) - g^{(\infty)}(x)]^2 \, dx \qquad (2)$$

Alternatively, one can monitor the end-to-end distance autocorrelation function of the time dependent distance $d(t)$

$$c(\Delta t) = \frac{\langle [d(t) - \bar{d}][d(t + \Delta t) - \bar{d}] \rangle_t}{\langle [d(t) - \bar{d}]^2 \rangle_t} \qquad (3)$$

Results and Discussion

General Considerations. A general overview of typical results from state of the art MD simulations applied to DME can be found in Figure 3, where the end-to-end distance distribution is displayed for simulations under conditions of vacuum, ES, and IS models, i.e., GBSW,[32,33] GBMV,[35,36] and FACTS.[37] It is not surprising that differences of DME conformations between explicit water and a vacuum are enormous (see dashed and solid lines in Figure 3A, respectively). But, conformational distributions of DME obtained with IS simulation conditions can still differ considerably from results of ES MD simulations. In particular, we observed that the most prominent TGT conformer is for all values of surface tension parameter γ less populated with IS than with ES simulation conditions (see Figure 3 and Figure S3, Supporting Information). With the IS model having positive surface energy, DME conformers are generally too compact due to the positive surface energy term and the unbalanced vdW attractive r^{-6} terms that preferentially populate the TGG′ and TGG conformers (see dotted line in Figure 3A and dotted lines in Figure S3, Supporting Information). Although the DME conformer distribution obtained with the IS model with positive surface energy

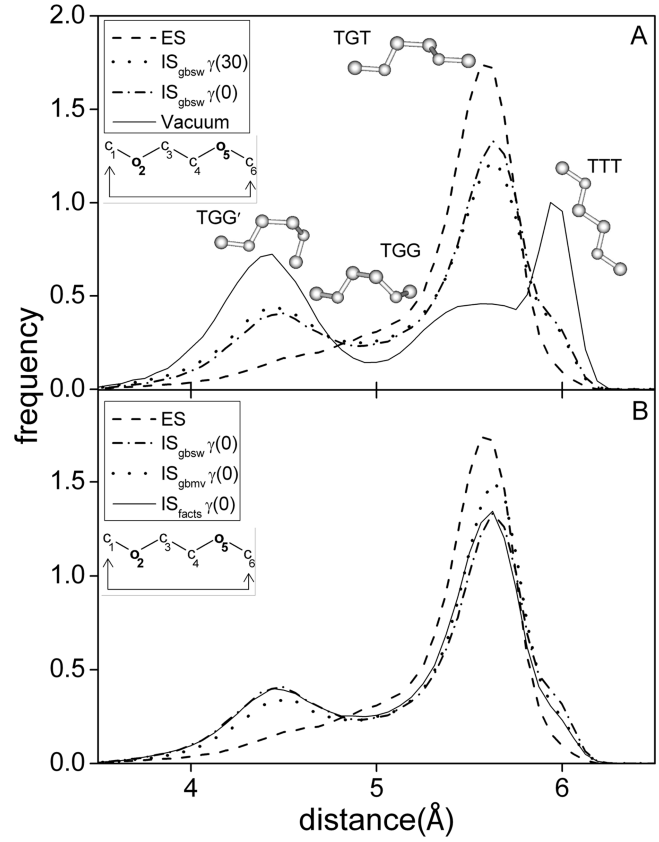

Figure 3. Conformational distribution of DME monitored by the C_1-C_6 end-to-end distance obtained from MD simulations under different force field conditions. (A) Comparison of ES results with data based on a vacuum and the IS GBSW model: vacuum conditions (solid line); explicit water (dashed line); IS GBSW with vanishing surface energy (dashed-dotted line); IS GBSW model with positive surface energy [$\gamma = 30$ cal/(mol Å^2)] (dotted line). (B) Comparison of ES results with three different IS models, all with a vanishing surface energy term: explicit water (dashed line); IS GBSW[32−34] (dashed-dotted line); IS GBMV[35,36] (dotted line); IS FACTS[37] (solid line).

shows large deviations relative to results from the ES model, the TGT conformer corresponding to the helix conformation of PEG (see Figure 2) remains the most populated one. Hence, the electrostatic screening effect due to an unspecific H-bond pattern of DME−water interactions, which is modeled by GB electrostatics, approximates qualitatively the most prominent features of the DME conformer distribution. The DME conformer distributions obtained with the IS GBSW model show compared to commonly used positive surface energies [$\gamma = 30$ cal/(mol Å^2)] relatively small variations for moderate negative surface energies [$\gamma = -15$ cal/(mol Å^2)] (see Figure S3A, Supporting Information). Under the same conditions, the other two IS models available in CHARMM (GBMV[35,36] and FACTS[37]) show comparatively larger variations (see Figure S3B and C of the Supporting Information).

In the following, we like to demonstrate what is responsible for the deficiencies of the IS GBSW model and how one can bridge the gap to reach better agreement with ES simulation data for DME and PEG. To optimize the energy function for the IS GBSW model, we first considered DME. For this purpose, we studied how the MD simulation data

for the IS GBSW DME model depend on the strength of the vdW attraction and the surface energy term. Next, we investigated how the IS GBSW DME model varies with the strength of specific Coulomb interactions. We optimized these above-mentioned interactions before we started to fine-tune the energy function with respect to the torsion potentials. Finally, we investigated whether the DME optimized energy function can be transferred to PEG.

As we will see later, a more accurate DME conformer distribution is obtained with an IS GBSW model with slightly reduced 1−4 Coulomb interactions, indicating a subtle but relevant contribution due to the specific H-bond pattern of water in the neighborhood of DME and PEG. This qualitatively correlates with earlier studies on the importance of the H-bond pattern between PEG and water that stabilizes the helical structure of PEG.[67−71]

Comparison of MD Simulation Data of DME with Explicit and Implicit Water Models and the Role of vdW Attraction and Surface Energy. We first like to compare MD simulation data of DME (see Figure 1), obtained with the ES and IS GBSW model with positive surface energy. Searching for a data representation, which shows the differences between the conventional ES and IS GBSW models most clearly, we found that this is the case for the end-to-end distance distributions of the DME atoms C_1 and C_6 (Figure 1). The dashed line in Figure 4 shows the distance distributions for the ES model and the dotted line for the IS GBSW model. One can clearly observe that, with the IS GBSW model, the compact DME structure at 4.5 Å is considerably more populated at the expense of the more extended structure at about 5.5 Å (see Figure 4A, dotted line compared to dashed line and schematic DME structures therein). Furthermore, in the IS GBSW model, a shoulder appears at 6.0 Å end-to-end distances, which is absent in the ES model. The enhanced occurrences of the compact structures in the IS GBSW model are due to unbalanced vdW interactions, as we will see.

One can qualitatively correct for the enhanced occurrence of compact structures by decreasing the attractive wing of the LJ interaction (except for the 1−4 atom pair interaction, which is part of the corresponding torsion potential and therefore should not be changed), or by decreasing the surface energy term into the negative regime as shown in the top and bottom parts of Figure 4, respectively. To account for unbalanced vdW interactions, negative surface energies were also considered to characterize the energetics of protein mutants.[23] However, negative surface energies were occasionally also used for IS GBSW models to account for dielectric screening, in the absence of more expensive electrostatic approaches like GB or PB.[24]

With extreme values of negative surface tension [$\gamma = -200$ cal/(mol Å^2)], the effect from the surface energy term saturates (Figure 4B). But, even with such extreme corrections, the end-to-end distance distribution of DME obtained with the IS GBSW model shows still marked deviations relative to the reference distribution obtained for conventional ES MD simulations (dashed line in Figure 4B): The side maximum at 4.5 Å remains, while it appears in the ES MD simulation as a shoulder only. Furthermore, a significant

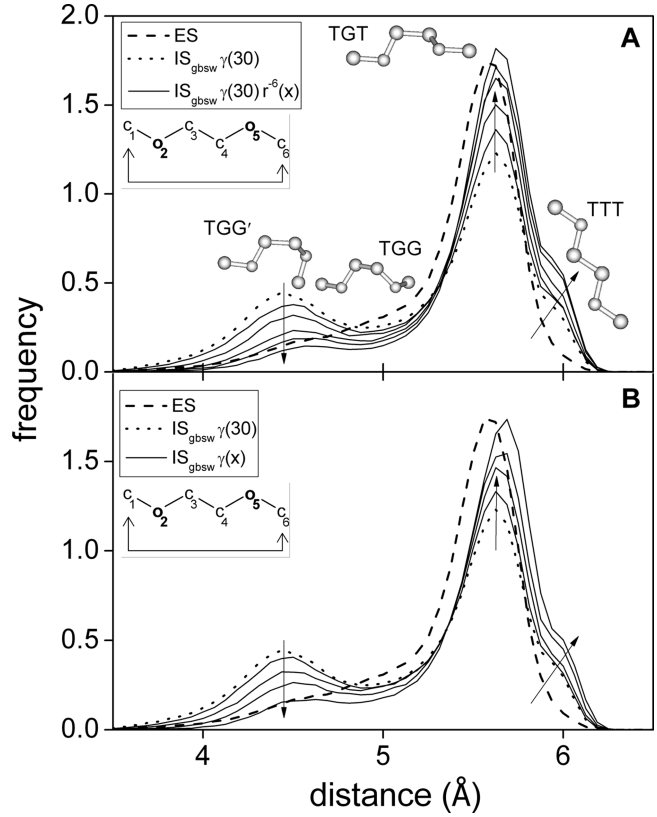

Figure 4. Role of attractive vdW and surface energy. The end-to-end distance distributions of DME obtained from MD simulation is shown for the ES (dashed line) and IS GBSW models with positive surface energy (dotted line). (A) The r^{-6} vdW attraction (except the 1−4 atom pair interaction) is scaled down by factors of 0.9, 0.7, 0.5, 0.3, and 0.1 (solid lines). The four most dominant DME structures are shown for the maxima at 4.5 and 5.5 Å and the shoulder at 6.0 Å, corresponding to structures where subsequent three torsion angles (C−O−C−C, O−C−C−O, C−O−C−C) correspond to TGT, TGG′, TGG, and TTT, respectively. (B) The surface tension coefficient γ is varied from 0, −50, −100, and −200, cal/(mol Å2) (solid lines). Note that for these exceedingly negative surface energies, variations of DME conformers can be observed also with the IS GBSW model favoring conformers with larger surfaces. The arrows indicate the direction of the changes in the distribution occurring by decreasing either the vdW attraction (A) or the surface tension coefficient (B).

shoulder appears at 6.0 Å, referring to the most extended DME structure (i.e., the TTT conformer), and the main maximum is shifted to larger distances. A similar behavior in the end-to-end distance distribution of DME is observed, if the attractive r^{-6} term of the vdW interaction is lowered from 1.0 by up to a factor of 0.1 (see Figure 4A).

Implicit Water Models of DME and the Role of 1−4 and 1−5 Coulomb Atom Pair Interactions. Exploring different options to improve the agreement of MD simulation data of DME, it turned out to be useful to first optimize the nonbonded interactions. Although the GB approach accounts for electrostatic contributions of solute−solvent interactions, there may be deficiencies, which need to be corrected. The strongest electrostatic interactions of DME and PEG involve ether oxygen pairs and ether oxygen with nonpolar hydrogens. Hence, we studied the dependence of the end-to-end

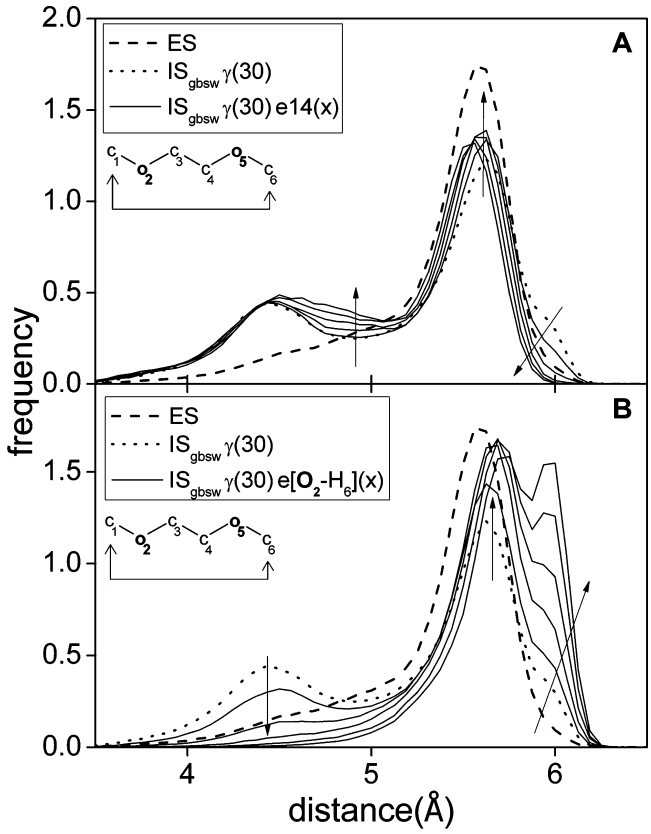

Figure 5. Role of 1−4 and 1−5 O−H atom pair interactions for the end-to-end distance distributions of DME obtained from MD simulation. In A and B, the dashed line refers to the ES and the dotted line to the IS GBSW model with positive surface energy. (A) The 1−4 atom pair Coulomb interaction is scaled down by factors of 0.9, 0.7, 0.5, 0.3, and 0.1 (solid lines). (B) The 1−5 oxygen−hydrogen (O_2-H_6, O_5-H_1) Coulomb interaction is scaled down by factors of 0.9, 0.7, 0.5, 0.3, and 0.1 (solid lines). The arrows indicate the direction of the changes in the distribution occurring by decreasing either the 1−4 atom pair (A) or the oxygen−hydrogen (B) electrostatic interaction.

distance distribution of DME on the Coulomb interactions of all 1−4 and oxygen−hydrogen 1−5 atom pairs (O−H; e.g., O_2-H_6 and O_5-H_1, where H_i is attached to C_i), shown in Figure 5 (solid lines), top and bottom parts, respectively. We suspected that the direct Coulomb interactions for these atom pairs may be overestimated. Therefore, they were scaled down by factors of 0.9, 0.7, 0.5, 0.3, and 0.1 (Figure 5).

Scaling down the 1−4 atom pair Coulomb interactions (Figure 5A) removes the shoulder at 6.0 Å and simultaneously can partially fill the valley between the side (at 4.5 Å) and main maximum (at 5.5 Å) of the end-to-end distance distribution. The former is mainly due to the 1−4 O−O electrostatic repulsion. Furthermore, while the height of the main maximum remains essentially invariant, its position is shifted slightly to lower distances. All these changes are useful to correct deficiencies that remained or appeared after diminishing vdW attraction or surface energy as discussed in the preceding subparagraph.

The 1−5 O−H interaction governs the strength of the weak H bond between O_2 (O_5) and the methyl group at position 6 (1). We also suspected that this direct 1−5 O−H interaction may be weaker in explicit solvent. Scaling down this interaction converts the side maximum at 4.5 Å to a shoulder similar to the ES model but of lower intensity. Simultaneously, the shoulder at 6.0 Å corresponding to all-trans stretched conformation (see Figure 5B) grows considerably, and the main maximum shifts to larger distances. Although the latter is unfavorable, in combination with the scaling of the 1−4 Coulomb interaction, it can be useful.

Implicit Water Models of DME: Fine-Tuning of Energy Function. The next step is to optimize the above-discussed four different nonbonded energy terms, which are (1) the attractive vdW term, (2) the surface energy, (3) the 1−4 atom pair Coulomb energy, and (4) the 1−5 O−H Coulomb energy. This was done in a tedious manual optimization procedure, where we first monitored the end-to-end distance distribution of DME (see Figure 6A). In doing so, we found two possible nearly equivalent solutions, which have in common that the interactions 3 and 4 are reduced to 90%. One option is with vanishing surface energy ($\gamma = 0$) where the vdW attractive r^{-6} term is reduced to 90% (red lines with open circles ○ in Figure 6). The second option is to assume a slightly repulsive surface energy term [$\gamma = -6$ cal/(mol Å^2)] with no change in the vdW attractive interaction (green lines with × in Figure 6). The corresponding end-to-end distance distributions are already close to the results obtained with the ES model (dashed line in Figure 6) that is used as a reference, but there is still room for improvement.

Alternatively to the reduction of specific Coulomb interactions as explained above (see also Table 1) to 90% of their original values, we lowered the Born radius of ether oxygen from 1.80 Å to 1.52 Å. The latter is the Born radius of backbone oxygen used in CHARMM.[94,95] Due to the stronger solvation of such oxygens, the corresponding explicit solute−solute interactions are effectively weakened, yielding better agreement with ES simulation data (see Figure S6 of the Supporting Information).

Optimization of the torsion potentials was done in the next step. For this purpose, we observed the free energy profiles of the torsion angles as derived from MD simulation data. We show the results of MD simulations for the torsion potentials involving rotations around the two C−O bonds and the C−C bond of DME in parts B and C of Figure 6, respectively. Most relevant is the C−C bond rotation, which shows still larger deviations from the MD simulation data obtained with the ES model (compare the dashed line with the green and red line in Figure 6C). Optimizing the parameters of the torsion potentials to the values given in Table 1, we obtain the black solid lines in Figure 6 marked with symbols ○ (×) referring to vanishing surface energy ($\gamma = 0$) and vdW attraction at 90% (negative surface energy [$\gamma = -6$ cal/(mol Å^2)] and unchanged vdW interaction). With this choice of the torsion potentials, we are essentially closing the gap appearing in the effective C−C bond torsion potential (Figure 6C) between the results of the ES reference model and the IS GBSW models. Slight improvements can also be observed for C−O torsion angle distribution and the end-to-end distance distribution (Figure 6A,B). The 1−5 O−C (O_2-C_6 and C_1-O_5) and the 1−4 O−O (O_2-O_5) and

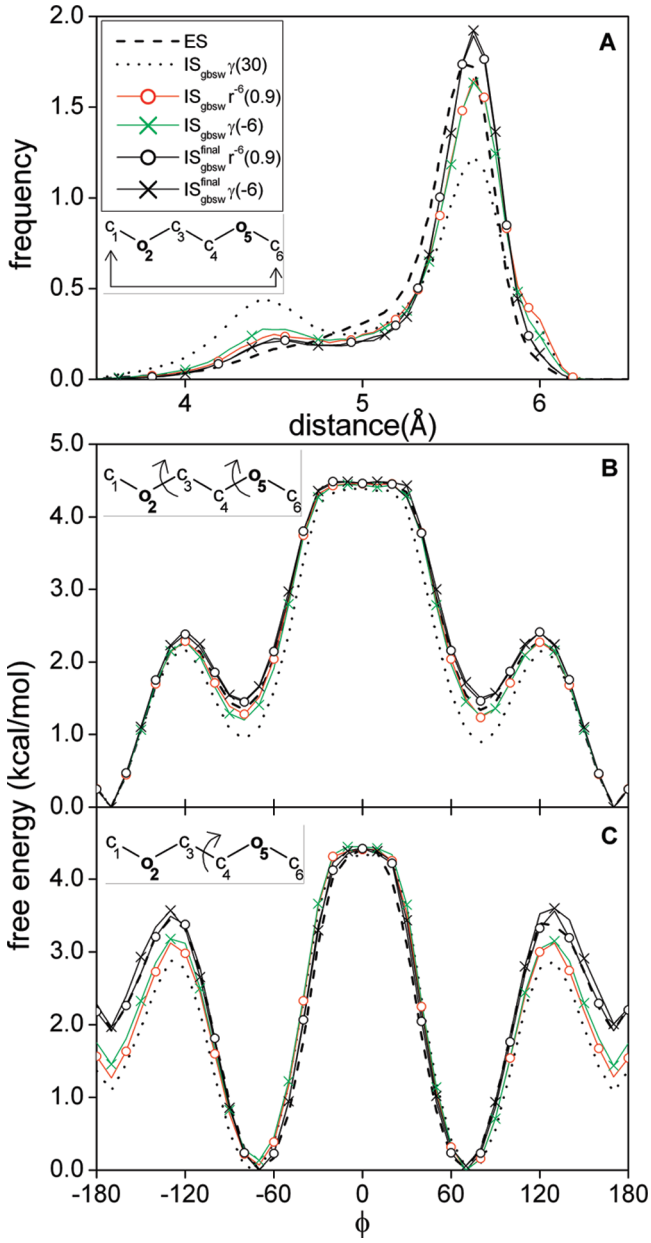

Figure 6. DME simulation data. Dashed (dotted) lines are the results based in the ES (IS GBSW with positive surface energy) model. All other data have in common that the 1−4 and 1−5 O−H atom pair Coulomb interactions are reduced to 90%. Red (green) lines with 'o' ('x') symbols display MD simulation data where the surface energy vanishes ($\gamma = 0$) and the attractive vdW interaction is reduced to 90% (the surface energy is negative [$\gamma = -6$ cal/(mol Å^2)] and the vdW interaction unchanged). The black solid lines show the final optimized MD simulation data including also the torsion potential corrections as described in the method section and Table 1. (A) End-to-end (C_1-C_6) distance distribution of DME. (B) Free energy profiles averaged over the two C−O−C−C torsion angles ($C_1-O_2-C_3-C_4$ and $C_3-C_4-O_5-C_6$). (C) Free energy profile of the O−C−C−O torsion angle ($O_2-C_3-C_4-O_5$). DME simulation data obtained by using the GB model only (IS with vanishing surface energy) are shown in Figures S4 and S5 of the Supporting Information.

distance distributions of DME are shown in Figure S4B and C of the Supporting Information, respectively. They also agree well with the MD simulation data of the ES model.

The force field parameters for the ES and IS GBSW model with positive surface energy and the two optimized IS GBSW models of DME are collected in Table 1. In the Supporting Information, we compare the populations of DME conformers obtained with the bare GB and the IS GBSW model with positive surface energy models for the atom pair distances (Figure S4, Supporting Information) and the torsion potentials (Figure S5, Supporting Information). These populations exhibit only moderate variations, since for moderate-sized surface tensions, the surface practically does not vary between the four most populated DME conformers (TGT, TGG′, TGG, TTT; see $G_{surface}$ values in Figure S1 of the Supporting Information).

MD Simulation of PEG in Implicit Solvent with the Fine-Tuned Energy Functions. We now explore whether the IS GBSW model developed for DME can be transferred to PEG. For this purpose, we compare MD simulation data of PEG6 (involving 6 monomer units) based on the ES model with data of PEG6 obtained with the two IS GBSW models that were optimized for DME.

We first analyze the local conformers of PEG6. The C_1-C_6 atom pair distance distributions of PEG6 (Figure S7A of the Supporting Information) are virtually identical to the corresponding end-to-end atom pair distribution of DME (compare Figure 6A). With the two optimized force fields, one obtains for PEG6 practically the same agreement with the data based on the ES model as for DME. The same is true for the distance distributions of 1−5 O−C (O_2-C_6) (Figure S7B of the Supporting Information) and 1−4 O−O (O_2-O_5) atom pairs (Figure S7C of the Supporting Information), where the corresponding distance distributions for DME are shown in Figure S4B and C of the Supporting Information. The torsion potentials obtained for PEG6 that correspond to the DME data shown in Figure 6B and C are displayed in Figure S8A and B of the Supporting Information. The corresponding distance distributions of PEG6 for more distant O−O atom pairs are shown in Figure S10 of the Supporting Information.

The global behavior of the PEG6 conformers is probed by the end-to-end C_1-C_{19} atom pair distance distribution. Agreement with the global behavior of conformers obtained with the ES model is much more demanding for the larger PEG6 chain molecules than for the small DME. Nevertheless, the agreement of the optimized IS GBSW models (Figure 7A, solid lines with ○ (×) symbols) is fairly good, while the IS GBSW model with positive surface energy fails (Figure 7A, dotted line).

To probe the generalities of our results found for PEG6 with the GBSW[32−34] model, we also explored the other two GB models available in CHARMM, i.e., GBMV[35,36] and FACTS,[37] using positive [$\gamma = 30$ cal/(mol Å^2)] and vanishing surface energies [$\gamma = 0$ cal/(mol Å^2)]. Under the same conditions, the GBMV model shows large variations for positive and vanishing surface energies. The latter is in good agreement with the ES results (Figure 7B). For DME (Figure S3B of Supporting Information), the corresponding structural variations obtained with GBMV are comparatively moderate.

On the other hand, the PEG6 end-to-end distance distribution obtained with FACTS shows only small variations (even smaller than they appear for DME; see Figure S3C of

Table 1. Force Field Parameters Used for DME with Explicit Solvent (ES) and Implicit Solvent (IS) GBSW Models

	CHARMM35 force field		adjusted CHARMM35 force field[a]	
force field term	ES	IS[b]	IS^{final}_r^{-6}(0.9)[b]	IS^{final}_γ(−6)[b]
C−O−C−C eq (1b)	0.29/2/0	0.29/2/0	0.20/2/0	0.20/2/0
O−C−C−O eq (1a)	0.59/1/180	0.59/1/180	1.09/1/180	1.09/1/180
vdW (no14)	1.0	1.0	0.9	1.0
e14fac	1.0	1.0	0.9	0.9
elec O(1)−H(6)	1.0	1.0	0.9	0.9
γ [cal/mol Å^2]	N/A	30	0	−6

[a] The two adjusted CHARMM35[93] ether force fields both involve down-scaling of 1−4 all atom and 1−5 O−H atom pair Coulomb interactions to 90% and optimized parameters of torsion potentials (see eqs 1a and 1b). The IS GBSW models IS^{final}_r^{-6}(0.9) and IS^{final}_γ(−6) force fields refer to the cases of (i) vanishing surface energy ($\gamma = 0$) and 90% of attractive vdW interaction and (ii) negative surface energy [$\gamma = -6$ cal/(mol Å^2)] and vdW interaction unchanged. [b] IS GBSW model.[32−34]

Supporting Information) with positive and vanishing surface energy terms and good agreement with the ES simulation data in both cases (Figure 7C). The insensitivity of FACTS on the variation of the surface energy in the end-to-end distance distribution of PEG6 as compared to a strong dependence found in the IS models of GBSW and GBMV may be related to the different way FACTS evaluates the effective molecular surface separating a low from a high dielectric medium. Naturally, the distributions of the local conformations of DME and consequently also of PEG do not agree so well for GBMV and FACTS, since they are not specifically optimized for DME and PEG, as it was done for the IS GBSW model in the present study.

While the maximum of the end-to-end distance distribution is at 13.5 Å for the ES model, it is only at 7 Å for the IS GBSW model with positive surface energy. The most probable distance of PEG6 in the ES model is considerably smaller than the end-to-end distance in the ideal TTT and TGT helix conformations, which are 24 Å and 18.5 Å, respectively. The distance of the energy minimized PEG6 helix conformer remains with about 17.2 Å for the IS GBSW model with positive surface energy and the optimized IS GBSW model close to value of the ideal helix structure of PEG. In addition to end-to-end distance distribution, the radius of gyration is also measured to assess the global structure of PEG6 and is shown in Figure S11 of the Supporting Information.

For the IS GBSW model with positive surface energy, the PEG6 conformers are generally much more compact due to the attractive surface energy term and the unbalanced vdW attractive r^{-6} terms that both predominantly populate the TGG′ and TGG conformers (see Figure 7A, dotted line). However, also the attractive Coulomb interactions of the 1−5 O−H atom pairs that preferentially populate the TGG′ state of DME (see insert in Figure 4A) may contribute to the more compact PEG6 conformers of the IS GBSW model with positive surface energy. One may suspect that it may also be favorable to reduce the Coulomb interactions for all atom pairs of the type 1−5 O−H to 90%. We tried it but obtained PEG6 conformers that were much too extended (results not shown). Hence, the best agreement with the ES model of PEG is obtained, if the force field optimized for the DME IS GBSW model is directly transferred to PEG.

Interestingly, the bare GB model without surface energy term applied to PEG6 yields an end-to-end distance distribution very close to the results obtained with the ES model (see Figure 7A, dashed-dotted line). However, the local PEG conformations obtained with the bare GB model differ from the ES model for both PEG6 and DME in the same way (compare Figures S7 and S8 as well as Figures S4 and S5, Supporting Information). Using small or nearly vanishing surface energies agrees with recent applications to compute solvation energies.[48−50,52,117]

Exploring the Conformational Space of PEG with MD Simulations. We evaluated the end-to-end distance autocorrelation functions of PEG6 according to eq 3, which exhibits a stretched exponential decay behavior $\exp(-t^{\beta})$ with $\beta = 2/3$ (Figure S12B of the Supporting Information) for the ES model, while for the IS GBSW models the decay behavior obeys a power law $t^{-\alpha}$ with $\alpha = 1/2$ (Figure S12A of the Supporting Information). A stretched exponential decay behavior with $\beta = 1/2$ was for instance also found for the Rouse polymer model in viscous media, which is typical for dynamics governed by defect diffusion.[118] Evidently the IS GBSW models show long-term dynamics, which differs from the dynamics of the ES model. The end-to-end distance autocorrelation function of PEG6 decays by 2 orders of magnitude in about 300 ps for the IS GBSW model and in about 1 ns for the ES model.

It is interesting to compare how efficient ES and IS GBSW models of PEG explore the conformational space with time. We expected that the behavior of the two models will differ, since in the absence of explicit solvent the dynamics of IS GBSW models are not slowed down by solvent viscosity. For that purpose, we monitored how the end-to-end distance distributions of PEG6 starting from the all trans stretched conformer approach the limit distribution of the ES model $g_{ES}^{(1\mu s)}(x)$ obtained with the maximum available time span of 1 μs. The time evolutions of the integral square deviations $[\Delta g^{(t)}]^2$, eq 2, from limit distribution $g_{ES}^{(1\mu s)}(x)$ are displayed in Figure 8 for the ES and IS GBSW models in a double logarithmic plot where the time decay appears approximately linear corresponding to a $t^{-\alpha}$ power law with $\alpha = 2/3$.

According to Figure 8, the end-to-end distance distribution of PEG6 seems to be converged after about 50 ns in the ES model (dashed line). At larger sampling times (t), $[\Delta g_{ES}^{(t)}]^2$ assumes a small plateau value with superimposed statistical fluctuations, since the ensemble of conformers is no longer large enough to exhibit further decay in $[\Delta g_{ES}^{(t)}]^2$. In the last 300 ns, $[\Delta g_{ES}^{(t)}]^2$ decays to zero, since the limit distribution $g_{ES}^{(1\mu s)}(x)$ representing the ensemble average is identical with the average using the maximum time span of 1 μs.

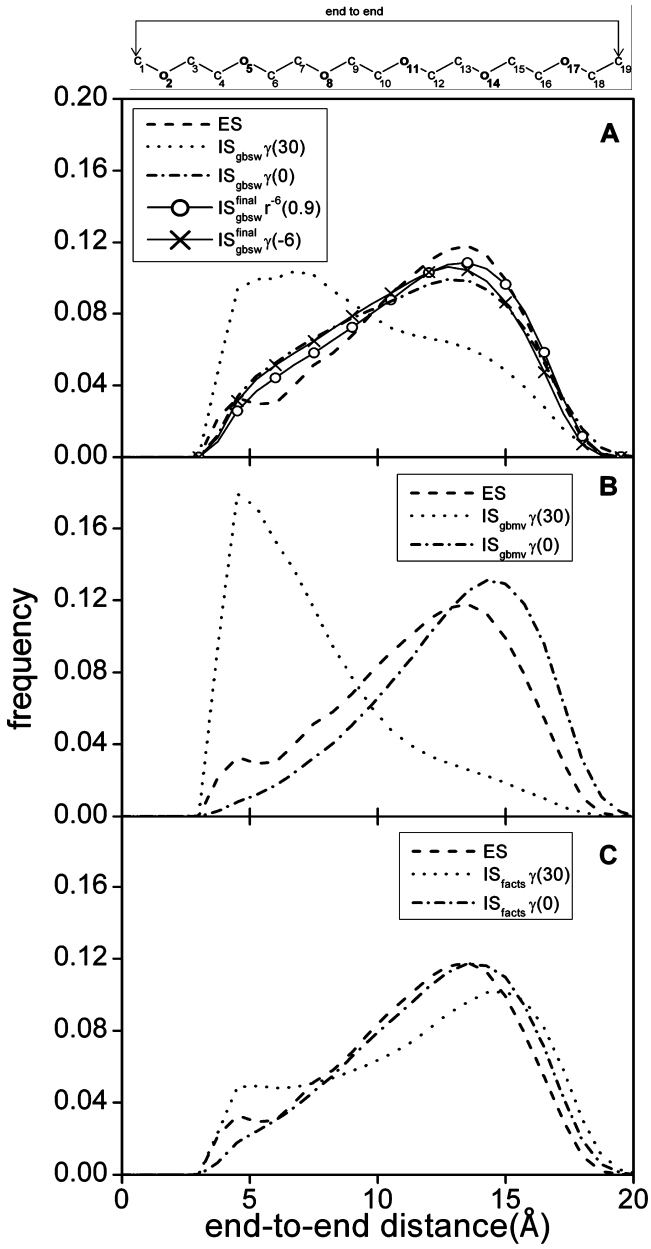

Figure 7. End-to-end (C_1-C_{19}) distance distributions for PEG6 obtained from MD simulation data with ES (1 μs) (dashed lines in parts A, B, C) and three IS models: (A) GBSW[32−34] (400 ns), (B) GBMV[35,36] (200 ns), and (C) FACTS[37] (400 ns) with varying surface energies, i.e., positive surface energy [$\gamma = 30$ cal/(mol Å^2)] (dotted lines), vanishing surface energy [$\gamma = 0$ cal/(mol Å^2)] (dashed-dotted lines). The solid lines in part A with ○ (×) symbols show the data from two optimized GBSW models (see Table 1).

The PEG6 conformer distributions that are based on the two IS GBSW models converge earlier at about 10 ns (solid lines in Figure 8). Beyond this time span until the maximum time span of 400 ns, the integral square deviations of the end-to-end distributions $[\Delta g^{(t)}_{IS}]^2$ are approximately constant at a low value that corresponds to small deviations of the limit distribution $g_{ES}^{(1\mu s)}(x)$ based on the ES model and the limit distributions $g_{IS}^{(0.4\mu s)}(x)$ based on the two optimized IS GBSW models. Hence, the dynamics of PEG6 with the IS GBSW model are about a factor of 5 faster than with the corresponding ES model, in agreement with MD simulations

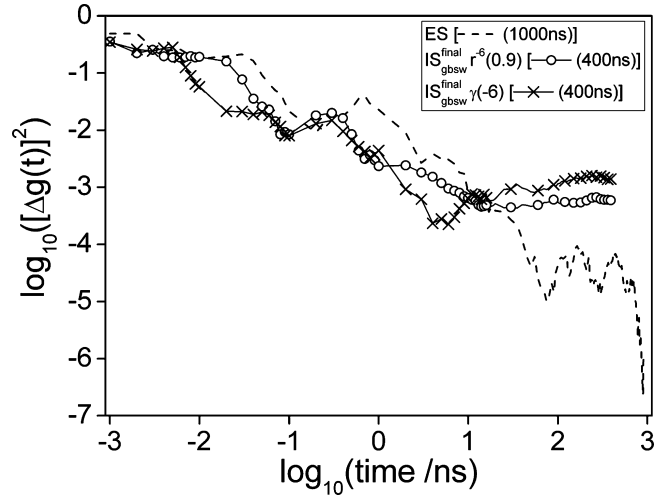

Figure 8. Efficiency of MD simulations to explore the conformational space of PEG6. Integral square deviation $[\Delta g^{(t)}]^2$, eq 2, of end-to-end atom pair distance distribution as a function of the time span used to obtain the ensemble average. Each time span starts at $t = 0$, where the initial PEG6 conformer is stretched all-trans. The lengths of the time spans to evaluate the averages of the distance distributions range from 1 ps to up to 1 μs. Dashed line displays $[\Delta g^{(t)}_{ES}]^2$ for the ES model. Solid lines show the time evolution of IS GBSW models with a maximum time span of 400 ns. The symbols ○ and × refer to the two optimized IS GBSW models (see Table 1). The reference distribution $g_{ES}^{(1\mu s)}(x)$ for all three cases considered here is taken from the ES model using the maximum time span of 1 μs. Additional trajectories of 50 ns time were generated for PEG6 with different seeds of the random number generator for both optimized IS GBSW models, which show similar behavior (Figure S13 of Supporting Information).

of different molecules using the IS GBMV model with a low friction coefficient.[27] The exploration of the PEG6 conformational space as probed by the end-to-end distance distributions is surprisingly slow compared to the behavior of the autocorrelation function of the same quantity, which decays by 2 orders of magnitude faster in about 1 ns and 300 ps for the ES and IS GBSW models, respectively (see Figure S12 of the Supporting Information).

Snapshots of the end-to-end distance distributions for different time spans are shown in Figure S14 (Supporting Information) for the ES model of PEG6 together with the final distribution for the time span of 1 μs. The end-to-end distance distribution of PEG6 obtained from MD simulation with the ES model where the 1 μs trajectory was split into 10 segments, each 0.1 μs long, is shown in Figure S15 of the Supporting Information.

Conclusions

Explicit solvent (ES) MD simulations are computationally expensive due to the large number of atom pair interactions, which need to be evaluated. Alternatively, one can perform MD simulations with an implicit solvent (IS) model that compromises between efficiency and accuracy. In an IS model, the electrostatic solute−solvent interactions are often modeled by simplified GB electrostatics, and the hydrophobic

effect is modeled by a surface energy term. The latter should generally favor compact solute conformers.

In MD simulations with an ES model, the attractive vdW interactions between solute atoms compete with corresponding interactions of solute−solvent atom pairs, leading thus to balanced and effectively weaker solute−solute interactions. For small molecular units like DME, the conformers vary only moderately but markedly with surface energy. More compact conformers are obtained with increasing surface energy for the IS GBSW and GBMV models, while with the IS FACTS model, the opposite behavior was observed. Comparing 1 μs MD simulation data of PEG with these three IS models, we found that the PEG conformers are much too compact for IS GBSW and GBMV models with positive surface energies. This phenomenon can be traced back to the lack of balance of attractive vdW interactions using these IS models with positive surface energy.

On the other hand, using these three GB models with vanishing surface energy yields PEG conformer distributions, which are globally realistic but may have some local deficiencies, which are similar as observed for DME. Adjusting the IS GBSW model to repair these deficiencies, it turned out that, in order to balance for a lack of solute−solvent attractive vdW interactions, the surface energy term must vanish and the attractive part of the vdW interactions must be reduced to 90% or alternatively, if the vdW interactions are not reduced, to use even a slightly negative surface energy. Hence, the influence from the unbalanced attractive vdW interactions is for PEG and DME even stronger than the hydrophobic effect. In addition, small but nevertheless significant reductions of the 1−4 and 1−5 O−H Coulomb interactions and adjustments of the torsion potentials were applied to obtain faithful local DME conformers. The former force field adjustments were necessary, since the IS GBSW model may have a tendency to overestimate Coulomb interactions at short distances. Interestingly, the force field originally adjusted for DME could be transferred to PEG unchanged.

The faithfulness of the PEG force field for an IS GBSW model developed in this contribution allows the study of entropy variations of PEG chain molecules under different geometry constraints (as for instance PEG bound with one or both ends on a wall or PEG moving through capillaries) most efficiently. For PEG6, the CPU time per time step is about a factor of 20 larger with the ES than with the IS GBSW model (see the discussion in the Supporting Information). MD simulations explore the conformational space of PEG6 in explicit and implicit water approximately according to a power law $t^{-\alpha}$ in time t with exponent $\alpha = 2/3$. The dynamics of the end-to-end distance distribution of PEG6 obey a stretched exponential decay law for the ES model, while a power law was found for the IS GBSW model, demonstrating differences in the long term behavior between these models. Due to the lack of viscosity in the IS GBSW model, the PEG6 conformations are explored about five times faster with the IS GBSW model than with the ES model. Hence, in total, exploration of the conformational space of PEG6 is for the IS GBSW model about a factor of 100 faster than for the ES model.

Acknowledgment. We thank Dr. Martin Karplus for providing the program CHARMM, and we thank ZEDAT for providing generous access to ABACUS4, the high performance computing facility at the Freie Universitaet Berlin. We gratefully acknowledge helpful discussions with Gernot Kieseritzky. This work was supported by the Deutsche Forschungsgemeinschaft (Sfb 765 Project C1).

Abbreviations. DME, 1,2-dimethoxy-ethane; ES, explicit solvent; FACTS, fast analytical continuum treatment of solvation; GB, generalized Born; GBMV, GB using molecular volume; GBSW, GB with a simple switching; IS, implicit solvent; LJ interaction, Lennard-Jones interaction; MD, molecular dynamics; PEG, polyethylene glycol; SA, solvent accessible surface area; TGT/TGG′/TGG/TTT/, conformers with three consecutive dihedral angles (C−O−C−C, O−C−C−O, and C−C−O−C) centered around either 180° for trans (T) or +60° (G) or −60° (G′) for gauche; vdW, van der Waals.

Supporting Information Available: Detailed description of explicit and implicit solvent simulation protocols; 2D structures of the 10 idealized DME and local PEG conformers; population of local DME conformers; End-to-end distance distribution of DME in IS_{gbsw}, IS_{gbmv}, IS_{facts}; atom pair distance distributions of DME and PEG6; average free energies of torsion angles (C−O−C−C and O−C−C−O) of DME and PEG6; Distance distribution of DME and PEG6 with different IS models; average O−O distance distribution of PEG6; radius of gyration obtained from MD simulations of PEG6; autocorrelation function and integral square deviation, eq 2, of end-to-end distance of PEG6; end-to-end distance distribution of PEG6 in explicit solvent. This material is available free of charge via the Internet at http://pubs.acs.org.

References

(1) Ben-Naim, A. Solvent Effects on Protein Stability and Protein Association. In *Protein-Solvent Interactions*, 1st ed.; Gregory, R. B., Ed.; Marcel Dekker, Inc.: New York, 1995; Vol. 592, pp 387−420.

(2) *Water: A Comprehensive Treatise*; Franks, F., Ed.; Plenum Pub Corp: New York, 1972−1982; Vol. 1−7.

(3) Eisenberg, D.; McLachlan, A. D. *Nature* **1986**, *319*, 199–203.

(4) Teeter, M. M. *Annu. Rev. Biophys. Biophys. Chem.* **1991**, *20*, 577–600.

(5) Soares, C. M.; Teixeira, V. H.; Baptista, A. M. *Biophys. J.* **2003**, *84*, 1628–1641.

(6) Privalov, P. L.; Makhatadze, G. I. *J. Mol. Biol.* **1993**, *232*, 660–679.

(7) Honig, B.; Yang, A.-S. Free Energy Balance in Protein Folding. In *Adv. Protein Chem.*; Anfinsen, C. B., Richards, F. M., Edsall, J. T., Eisenberg, D. S., Eds.; Academic Press: San Diego, 1995; Vol. 46, pp 27−58.

(8) Klebe, G. *Drug Discovery Today* **2006**, *11*, 580–594.

(9) Corbeil, C. R.; Moitessier, N. *J. Chem. Inf. Model.* **2009**, *49*, 997–1009.

(10) Froloff, N.; Windemuth, A.; Honig, B. *Protein Sci.* **1997**, *6*1293–1301.

(11) Frauenfelder, H.; Fenimore, P. W.; Chen, G.; McMahon, B. H. *Proc. Natl. Acad. Sci. U. S. A.* **2006**, *103*, 15469–15472.

(12) Dill, K. A. *Biochemistry* **2002**, *29*, 7133–7155.

(13) Ben-Naim, A. *Hydrophobic Interactions*; Plenum Press: New York: 1980.

(14) Vaitheeswaran, S.; Yin, H.; Rasaiah, J. C.; Hummer, G. *Proc. Natl. Acad. Sci. U. S. A.* **2004**, *101*, 17002–17005.

(15) Southall, N. T.; Dill, K. A.; Haymet, A. D. J. *J. Phys. Chem. B* **2001**, *106*, 521–533.

(16) Makarov, V. A.; Feig, M.; Andrews, B. K.; Pettitt, B. M. *Biophys. J.* **1998**, *75*, 150–158.

(17) Knapp, E. W.; Muegge, I. *J. Phys. Chem.* **1993**, *97*, 11339–11343.

(18) Warwicker, J.; Watson, H. C. *J. Mol. Biol.* **1982**, *157*, 671–679.

(19) Cramer, C. J.; Truhlar, D. G. *Chem. Rev.* **1999**, *99*, 2161–2200.

(20) Roux, B.; Simonson, T. *Biophys. Chem.* **1999**, *78*, 1–20.

(21) Gilson, M. K.; Davis, M. E.; Luty, B. A.; McCammon, J. A. *J. Phys. Chem.* **1993**, *97*, 3591–3600.

(22) Baker, N. A. *Curr. Opin. Struct. Biol.* **2005**, *15*, 137–143.

(23) Lopes, A.; Alexandrov, A.; Bathelt, C.; Archontis, G.; Simonson, T. *Proteins: Struct., Funct., Bioinf.* **2007**, *67*, 853–867.

(24) Ferrara, P.; Apostolakis, J.; Caflisch, A. *Proteins: Struct., Funct., Bioinf.* **2002**, *46*, 24–33.

(25) Chen, J.; Brooks, C. L. *Phys. Chem. Chem. Phys.* **2008**, *10*, 471–481.

(26) Vorobjev, Y. N.; Almagro, J. C.; Hermans, J. *Proteins: Struct., Funct., Bioinf.* **1998**, *32*, 399–413.

(27) Feig, M. *J. Chem. Theory Comput.* **2007**, *3*, 1734–1748.

(28) Warshel, A.; Aqvist, J. *Annu. Rev. Biophys. Biophys. Chem.* **1991**, *20*, 267–298.

(29) Kauzmann, W. Some Factors in the Interpretation of Protein Denaturation. In *Adv. Protein Chem.*; Anfinsen, C. B., Anson, M. L., Bailey, K., Edsall, J. T., Eds.; Academic Press: New York, 1959; Vol. 14, pp 1−63.

(30) Tanford, C. Protein Denaturation. In *Adv. Protein Chem.*; Anfinsen, C. B., Anson, M. L., Edsall, J. T., Frederic, M. R., Eds.; Academic Press: New York, 1968; Vol. 23, pp 121−282.

(31) Hummer, G.; Garde, S.; García, A. E.; Pohorille, A.; Pratt, L. R. *Proc. Natl. Acad. Sci. U. S. A.* **1996**, *93*, 8951–8955.

(32) Im, W.; Lee, M. S.; Brooks, C. L. *J. Comput. Chem.* **2003**, *24*, 1691–1702.

(33) Im, W.; Feig, M.; Brooks, C. L. *Biophys. J.* **2003**, *85*, 2900–2918.

(34) Chen, J.; Im, W.; Brooks, C. L. *J. Am. Chem. Soc.* **2006**, *128*, 3728–3736.

(35) Lee, M. S.; Salsbury, J. F. R.; Brooks, C. L., III *J. Chem. Phys.* **2002**, *116*, 10606–10614.

(36) Lee, M. S.; Feig, M.; Salsbury, F. R.; Brooks, C. L. *J. Comput. Chem.* **2003**, *24*, 1348–1356.

(37) Haberthür, U.; Caflisch, A. *J. Comput. Chem.* **2008**, *29*, 701–715.

(38) Feig, M.; Onufriev, A.; Lee, M. S.; Im, W.; Case, D. A.; Brooks, C. L. *J. Comput. Chem.* **2004**, *25*, 265–284.

(39) Im, W.; Beglov, D.; Roux, B. *Comput. Phys. Commun.* **1998**, *111*, 59–75.

(40) Still, W. C.; Tempczyk, A.; Hawley, R. C.; Hendrickson, T. *J. Am. Chem. Soc.* **1990**, *112*, 6127–6129.

(41) Lazaridis, T.; Karplus, M. *Proteins: Struct., Funct., Bioinf.* **1999**, *35*, 133–152.

(42) Feig, M.; Brooks, C. L. *Curr. Opin. Struct. Biol.* **2004**, *14*, 217–224.

(43) Chen, J.; Brooks, C. L.; Khandogin, J. *Curr. Opin. Struct. Biol.* **2008**, *18*, 140–148.

(44) Tomasi, J. *Theor. Chem. Acc.* **2004**, *112*, 184–203.

(45) Lee, B.; Richards, F. M. *J. Mol. Biol.* **1971**, *55*, 379–400.

(46) Richmond, T. J. *J. Mol. Biol.* **1984**, *178*, 63–89.

(47) Fraczkiewicz, R.; Braun, W. *J. Comput. Chem.* **1998**, *19*, 319–333.

(48) Onufriev, A.; Case, D. A.; Bashford, D. *J. Comput. Chem.* **2002**, *23*, 1297–1304.

(49) Zhu, J.; Shi, Y.; Liu, H. *J. Phys. Chem. B* **2002**, *106*, 4844–4853.

(50) Mongan, J.; Simmerling, C.; McCammon, J. A.; Case, D. A.; Onufriev, A. *J. Chem. Theory Comput.* **2007**, *3*, 156–169.

(51) Spassov, V. Z.; Yan, L.; Szalma, S. *J. Phys. Chem. B* **2002**, *106*, 8726–8738.

(52) Wagoner, J. A.; Baker, N. A. *Proc. Natl. Acad. Sci. U. S. A.* **2006**, *103*, 8331–8336.

(53) Gallicchio, E.; Kubo, M. M.; Levy, R. M. *J. Phys. Chem. B* **2000**, *104*, 6271–6285.

(54) Floris, F.; Tomasi, J. *J. Comput. Chem.* **1989**, *10*, 616–627.

(55) Pitera, J. W.; van Gunsteren, W. F. *J. Am. Chem. Soc.* **2001**, *123*, 3163–3164.

(56) Gallicchio, E.; Levy, R. M. *J. Comput. Chem.* **2004**, *25*, 479–499.

(57) Cheatham Iii, T. E.; Kollman, P. A. *Annu. Rev. Phys. Chem.* **2003**, *51*, 435–471.

(58) Bailey, F. E.; Koleske, J. V. *Poly(ethylene oxide)*; Academic Press: New York, 1976.

(59) *Poly(Ethylene Glycol) Chemistry: Biotechnical and Biomedical Applications*; Harris, J. M., Ed.; Plenum Publishing: New York, 1992.

(60) Takahashi, Y.; Tadokoro, H. *Macromolecules* **1973**, *6*, 672–675.

(61) Matsuura, H.; Miyazawa, T. *J. Polym. Sci. A-2* **1969**, *7*, 1735–1744.

(62) Mueller-Plathe, F.; van Gunsteren, W. F. *Macromolecules* **1994**, *27*, 6040–6045.

(63) Liu, H.; Müller-Plathe, F.; van Gunsteren, W. F. *J. Chem. Phys.* **1995**, *102*, 1722–1730.

(64) Goutev, N.; Ohno, K.; Matsuura, H. *J. Phys. Chem. A* **2000**, *104*, 9226–9232.

(65) Yoshida, H.; Kaneko, I.; Matsuura, H.; Ogawa, Y.; Tasumi, M. *Chem. Phys. Lett.* **1992**, *196*, 601–606.

(66) Tasaki, K.; Abe, A. *Polym. J.* **1985**, *17*, 641–655.

(67) Lusse, S.; Arnold, K. *Macromolecules* **1996**, *29*, 4251–4257.

(68) Wang, R. L. C.; Kreuzer, H. J.; Grunze, M. *J. Phys. Chem. B* **1997**, *101*, 9767–9773.

(69) Tasaki, K. *J. Am. Chem. Soc.* **1996**, *118*, 8459–8469.

(70) Depner, M.; Schürmann, B. L.; Auriemma, F. *Mol. Phys.* **1991**, *74*, 715–733.

(71) Heymann, B.; Grubmüller, H. *Chem. Phys. Lett.* **1999**, *307*, 425–432.

(72) Pasut, G.; Guiotto, A.; Veronese, F. *Expert Opin. Ther. Pat.* **2004**, *14*, 859–894.

(73) Mero, A.; Schiavon, O.; Pasut, G.; Veronese, F. M.; Emilitri, E.; Ferruti, P. *J. Bioact. Compat. Polym.* **2009**, *24*, 220–234.

(74) Fuertges, F.; Abuchowski, A. *J. Controlled Release* **1990**, *11*, 139–148.

(75) Harris, J. M.; Chess, R. B. *Nat. Rev. Drug Discovery* **2003**, *2*, 214–221.

(76) Lascombe, M.-B.; Milat, M.-L.; Blein, J.-P.; Panabières, F.; Ponchet, M.; Prangé, T. *Acta Crystallogr., Sect. D* **2000**, *56*, 1498–1500.

(77) Herrmann, A.; Arnold, K.; Pratsch, L. *Biosci. Rep.* **1985**, *5*, 689–696.

(78) Zimmerberg, J.; Parsegian, V. A. *Nature* **1986**, *323*, 36–39.

(79) O'Riordan, C. R.; Lachapelle, A.; Delgado, C.; Parkes, V.; Wadsworth, S. C.; Smith, A. E.; Francis, G. E. *Hum. Gene Ther.* **1999**, *10*, 1349–1358.

(80) Prime, K. L.; Whitesides, G. M. *J. Am. Chem. Soc.* **1993**, *115*, 10714–10721.

(81) Pertsin, A. J.; Grunze, M.; Garbuzova, I. A. *J. Phys. Chem. B* **1998**, *102*, 4918–4926.

(82) Harder, P.; Grunze, M.; Dahint, R.; Whitesides, G. M.; Laibinis, P. E. *J. Phys. Chem. B* **1998**, *102*, 426–436.

(83) Veronese, F.; Harris, J. M. *Adv. Drug Delivery Rev.* **2002**, *54*, 453–456.

(84) Roberts, M. J.; Bentley, M. D.; Harris, J. M. *Adv. Drug Delivery Rev.* **2002**, *54*, 459–476.

(85) Guillaudeu, S. J.; Fox, M. E.; Haidar, Y. M.; Dy, E. E.; Szoka, F. C.; Fréchet, J. M. J. *Bioconjugate Chem.* **2008**, *19*, 461–469.

(86) Veronese, F.; Pasut, G. *Drug Discovery Today* **2005**, *10*, 1451–1458.

(87) Mammen, M.; Choi, S.-K.; Whitesides, G. M. *Angew. Chem., Int. Ed.* **1998**, *37*, 2754–2794.

(88) Kramer, R. H.; Karpen, J. W. *Nature* **1998**, *395*, 710–713.

(89) Diestler, D. J.; Knapp, E. W. *Phys. Rev. Lett.* **2008**, *100*, 178101–4.

(90) Diestler, D. J.; Knapp, E. W. *J. Phys. Chem. C* **2009**.

(91) Oesterhelt, F.; Rief, M.; Gaub, H. E. *New J. Phys.* **1999**, *1*, 6.16.11.

(92) Vorobyov, I.; Anisimov, V. M.; Greene, S.; Venable, R. M.; Moser, A.; Pastor, R. W.; Alexander, D.; MacKerell, J. *J. Chem. Theory Comput.* **2007**, *3*, 1120–1133.

(93) Lee, H.; Venable, R. M.; MacKerell, A. D.; Pastor, R. W. *Biophys. J.* **2008**, *95*, 1590–1599.

(94) Brooks, B. R.; Brooks, C. L.; MacKerell, A. D. J.; Nilsson, L.; Petrella, R. J.; Roux, B.; Won, Y.; Archontis, G.; Bartels, C.; Boresch, S.; Caflisch, A.; Caves, L.; Cui, Q.; Dinner, A. R.; Feig, M.; Fischer, S.; Gao, J.; Hodoscek, M.; Im, W.; Kuczera, K.; Lazaridis, T.; Ma, J.; Ovchinnikov, V.; Paci, E.; Pastor, R. W.; Post, C. B.; Pu, J. Z.; Schaefer, M.; Tidor, B.; Venable, R. M.; Woodcock, H. L.; Wu, X.; Yang, W.; York, D. M.; Karplus, M. *J. Comput. Chem.* **2009**, *30*, 1545–1614.

(95) MacKerell, A. D. J.; Bashford, D.; Bellott, M. R. L.; Dunbrack, J.; Evanseck, J. D.; Field, M. J.; Fischer, S.; Gao, J.; Guo, H.; Ha, S.; Joseph-McCarthy, D.; Kuchnir, L.; Kuczera, K.; Lau, F. T. K.; Mattos, C.; Michnick, S.; Ngo, T.; Nguyen, D. T.; Prodhom, B.; W. E.; Reiher, I.; Roux, B.; Schlenkrich, M.; Smith, J. C.; Stote, R.; Straub, J.; Watanabe, M.; Wiórkiewicz-Kuczera, J.; Yin, D.; Karplus, M. *J. Phys. Chem. B* **1998**, *102*, 3586–3616.

(96) Neyertz, S.; Brown, D.; Thomas, J. O. *J. Chem. Phys.* **1994**, *101*, 10064–10073.

(97) Smith, G. D.; Jaffe, R. L.; Yoon, D. Y. *J. Phys. Chem.* **1993**, *97*, 12752–12759.

(98) Smith, G. D.; Jaffe, R. L.; Yoon, D. Y. *J. Am. Chem. Soc.* **1995**, *117*, 530–531.

(99) Bedrov, D.; Borodin, O.; Smith, G. D. *J. Phys. Chem. B* **1998**, *102*, 5683–5690.

(100) Masatoki, S.; Takamura, M.; Matsuura, H.; Kamogawa, K.; Kitagawa, T. *Chem. Lett.* **1995**, *24*, 991–992.

(101) Begum, R.; Sagawa, T.; Masatoki, S.; Matsuura, H. *J. Mol. Struct.* **1998**, *442*, 243–250.

(102) Born, M. *Z. Phys.* **1920**, *1*, 45–48.

(103) Edinger, S. R.; Cortis, C.; Shenkin, P. S.; Friesner, R. A. *J. Phys. Chem. B* **1997**, *101*, 1190–1197.

(104) Dominy, B. N.; Brooks, C. L. *J. Phys. Chem. B* **1999**, *103*, 3765–3773.

(105) Bashford, D.; Case, D. A. *Annu. Rev. Phys. Chem.* **2000**, *51*, 129–152.

(106) Wesson, L.; Eisenberg, D. *Protein Sci.* **1992**, *1*, 227–235.

(107) Weiner, S. J.; Kollman, P. A.; Nguyen, D. T.; Case, D. A. *J. Comput. Chem.* **1986**, *7*, 230–252.

(108) Case, D. A.; Darden, T.; Gohlke, H.; Luo, R. K. M. M.; Onufriev, A.; Simmerling, C.; Wang, B.; Woods, R. J. *J. Comput. Chem.* **2005**, *26*, 1668–1688.

(109) Jorgensen, W. L.; Chandrasekhar, J.; Madura, J. D.; Impey, R. W.; Klein, M. L. *J. Chem. Phys.* **1983**, *79*, 926–935.

(110) Hermann, R. B. *J. Phys. Chem.* **1972**, *76*, 2754–2759.

(111) Durell, S. R.; Brooks, B. R.; Ben-Naim, A. *J. Phys. Chem.* **1994**, *98*, 2198–2202.

(112) Phillips, J. C.; Braun, R.; Wang, W.; Gumbart, J.; Tajkhorshid, E.; Villa, E.; Chipot, C.; Skeel, R. D.; Kalé, L.; Schulten, K. *J. Comput. Chem.* **2005**, *26*, 1781–1802.

(113) Darden, T.; York, D.; Pedersen, L. *J. Chem. Phys.* **1993**, *98*, 10089–10092.

(114) Nina, M.; Im, W.; Roux, B. *Biophys. Chem.* **1999**, *78*, 89–96.

(115) Nosé, S.; Klein, M. L. *J. Chem. Phys.* **1983**, *78*, 6928–6939.

(116) Hoover, W. G. *Phys. Rev. A* **1985**, *31*, 1695–1697.

(117) Sitkoff, D.; Sharp, K. A.; Honig, B. *J. Phys. Chem.* **1994**, *98*, 1978–1988.

(118) Knapp, E. W. *J. Comput. Chem.* **1992**, *13*, 793–798.

CT100075M